




Effect of SILAR cycle on gas sensing properties of In₂O₃ thin films for CO gas sensor

Banu Horoz¹, Sümeyra Tuna Yıldırım², Baktiyar Soltabayev³, Aytunç Ateş⁴, Selim Acar⁵, and M. Ali Yıldırım^{1,*} 

¹ Department of Electrical and Electronics Engineering, Engineering- Architecture Faculty, Erzincan Binali Yıldırım University, Erzincan, Turkey

² Department of Analytical Chemistry, Pharmacy Faculty, Erzincan Binali Yıldırım University, Erzincan, Turkey

³ National Laboratory Astana, Nazarbayev University, Nur-Sultan, Kazakhstan

⁴ Department of Material Engineering, Engineering and Natural Sciences Faculty, Ankara Yıldırım Beyazıt University, Ankara, Turkey

⁵ Department of Physics, Science Faculty, Gazi University, Ankara, Turkey

Received: 25 May 2023

Accepted: 5 January 2024

Published online:
17 January 2024

© The Author(s), 2024

ABSTRACT

In₂O₃ thin films were deposited via Successive Ionic Layer Adsorption and Reaction (SILAR) method on glass substrates at 20, 30, 40, and 50 SILAR cycles. The effect of SILAR cycle on the general and CO gas sensing properties of the films was investigated. The GIXRD and FE-SEM results indicated that the films had cubic phase and porous morphology. As a function of temperature and gas concentration, CO gas sensing measurements of In₂O₃ thin film-based sensors were made, and the detection limit and operating temperature values were determined. The optimal operating temperature was found to be 222 °C for all sensors. The CO sensing results demonstrated that the sensor with 30 SILAR cycle had higher sensitivity for 1–100-ppm gas concentration values at 222 °C operating temperature than the others. The sensing responses of the sensors increased from 12 to 29% for 1-ppm CO gas and from 52 to 91% for 100-ppm CO gas at 222 °C, depending on the SILAR cycle. The detection limit of the sensors toward CO gas at 222 °C reached 1 ppm, and the response and recovery times of the sensor with 30 SILAR cycle were found to be 54.2 s and 49 s for 1-ppm CO, and 47.4 and 62.5 s for 100-ppm CO gas at 222 °C, respectively. The activation energy (E_a) values of the sensors were found to change between 0.08 and 0.15 eV in the temperature range of 300–340 K and between 0.700 and 0.749 eV in the temperature range of 350–520 K, with SILAR cycle number. Finally, in this study, it was revealed that SILAR cycle number changed the structural, morphological, and CO gas sensing properties of the In₂O₃ thin films, and SILAR cycle optimization was performed for the highly sensitive In₂O₃ thin film-based CO gas sensor.

Address correspondence to E-mail: mayildirim@erzincan.edu.tr

1 Introduction

As our world has become more automated, the size of global gas sensor market is predicted to reach US\$5.6 billion industry by 2024 [1]. Introducing new products and/or improving existing sensing materials along with the recent technological developments will significantly affect the growth in this industry. Metal oxides are one of the most popular materials used for detecting flammable, toxic, and explosive gases known as detection materials and have extensively been researched for detecting more than 150 hazardous gases [2]. Metal oxide-based gas sensors have superior success in detecting hazardous gases due to the advantages, such as simple design, compact size, low cost, low power consumption, fast response time, and high sensitivity. Nevertheless, the superior success attributed to gas sensing using metal oxides is considerable mostly at high temperatures (> 150 °C), indicating the need for additional heater and circuitry in the sensor setup. Thus, this leads to higher costs, high power consumption, more complexity, and complex integration [3, 4]. Using nanostructured metal oxides is a good approach to partially overcome above-mentioned shortages associated with metal oxide-based gas sensors. Especially, they can have higher sensitivity to very low gas concentrations at lower temperatures and better selectivity compared to their bulk equivalents. Also, one of the most important factors in increasing the performance of metal oxides is the reduction of particle size to nanoscale. Nanostructured metal oxides have large surface area due to the reduction of particle size to nanoscale, so more adsorption of gaseous species takes place, resulting in improved gas detection performance of the sensor [4].

Nanostructured metal oxides are very suitable materials for toxic gas sensing due to their low cost, facile synthesis, and high response to target gas. Common n-type-nanostructured metal oxides used to fabricate gas sensors for detection of toxic gases are SnO_2 , ZnO , WO_3 , and In_2O_3 . Of these nanostructured metal oxides, In_2O_3 is n-type metal oxide semiconductor with a wide direct band gap (3.55–3.75 eV) [5, 6]. In_2O_3 -nanostructured thin films can be used for designing ultra-sensitive sensors due to their high electrical conductivity and intrinsic oxygen vacancy [6–8]. Also, crystal structure and surface morphology have a significant effect on the sensing performance of In_2O_3 nanomaterials. For this reason, different In_2O_3 nanostructures such as nanoparticles

[9], nanorods and nanowires [10], nanosheets or nanoplates [11], and 3D hierarchitectures [12, 13] have been fabricated for meeting the demand for practical applications. Recently, significant efforts have been made to address the methods of structural design and controllable synthesis for building portable and reliable In_2O_3 -based sensors to satisfy the standard in many applications, such as the chemical, pharmaceutical, and food industries [14, 15].

For the deposition of nanostructured thin films, simple, low cost, efficient, and easy to control techniques/methods that guarantee reproducible experimental results are preferred. The SILAR method is one of the simple, cost-effective, reproducible, and efficient chemical methods used for the deposition of nanostructured thin films, in which the film thickness is controlled depending on the cycle number. The spin coating method is another widely used simple and low-cost deposition method operating at low temperatures and in solution phase. SILAR and spin coating methods allow the possibility for deposition films with controllable thickness and also offer the advantage to produce films on a large substrate surface. The possibility to control the deposition and film thickness more precisely in the SILAR method due to the sequential deposition, the need for no device or expensive equipment for thin-film deposition, and the ability to use more than one substrate at a time are the main advantages of SILAR method as compared with the spin coating method [16, 17]. In SILAR method, thin films can be kept at room temperature without needing quality substrates and vacuum. There is minimal waste of chemicals when compared with other chemical and physical methods [18, 19]. Also, In the SILAR method especially the structural and morphological properties of thin films can change depending on growth parameters, such as precursors, concentration of precursors, counterions, pH of precursor solutions, adsorption, reaction, and rinsing time. The thin films deposited via the SILAR method can be re-deposited by keeping the deposition parameters and deposition conditions constant.

In this study, producing In_2O_3 thin films in different SILAR cycles with SILAR method and the effects of SILAR cycle number on the general and CO gas sensing properties of In_2O_3 thin films were primarily focused. By determining these effects, SILAR cycle optimization was performed for the highly sensitive In_2O_3 thin film-based CO gas sensor.

2 Experimental procedure

2.1 Deposition of In₂O₃ thin films

In₂O₃ thin films were successfully deposited via SILAR method on glass substrates at room temperature and 20, 30, 40, and 50 SILAR cycles. For deposition of In₂O₃ thin films, aqueous indium–ammonia complex ([In(NH₃)₄]³⁺) was chosen for the cation precursor, in which analytical reagents of 0.1-M InCl₃ (pH ≈ 5.5, %98 Sigma-Aldrich) and aqueous ammonia solution (NH₃–25–30%-Sigma-Aldrich) were used. For preparing the [In(NH₃)₄]³⁺ complex, aqueous ammonia solution was added into 0.1-M InCl₃ (pH ≈ 5.5) solution until the pH value of this solution was 10. For synthesis of In₂O₃ thin films, one SILAR cycle consisted of the four following steps: (1) immersing the substrate in the aqueous ([In(NH₃)₄]³⁺ complex for 20 s to create a thin liquid film containing ([In(NH₃)₄]³⁺ complex ions on the substrate; (2) immersing immediately the withdrawn substrates in hot water (90 °C) for 7 s to form an In₂O₃ layer; (3) drying the substrate in the air for 60 s; and (4) rinsing the substrate in a separate beaker for 20 s to remove large and loosely bonded In₂O₃ species. Thus, one SILAR cycle of In₂O₃ deposition was completed. The adsorption, reaction, and rinsing times were chosen experimentally so that deposition occurred layer wise and resulted in the homogeneous thin-film structure. The detail information about the SILAR cycle and In₂O₃ thin-film deposition via the SILAR method was reported in our previous studies [18, 19]. All the films were deposited repeating 20, 30, 40, and 50 SILAR cycles. Using a PHE 102 Spectroscopic Ellipsometer, the thicknesses of the films were found to be 74 ± 2.54, 115 ± 3.11, 132 ± 3.61, and 148 ± 3.83 nm for 20, 30, 40, and 50 SILAR cycles, respectively.

Firstly, structural, morphological, and compositional characterizations of In₂O₃ thin films were performed. After then, the interdigitated (IDT) silver (Ag) electrodes for In₂O₃ thin film-based sensors were coated by thermal evaporation on the films using Ag metal (99.9%, Sigma-Aldrich) and a shadow mask with an interlinked electrode width of 45 μm, length of 2.5 mm, and spacing of 90 μm. The main reasons for choosing Ag electrodes are their good catalytic effect, good bond strength, being widely used, the practicality of evaporation for electrode fabrication,

and their very cost-effectiveness compared to Au and Pt electrodes.

2.2 Characterization methods

GIXRD, FE-SEM, EDAX, and gas sensing measurements were performed to investigate the effect of SILAR cycle number on the structural, morphological, compositional, and CO gas sensing properties of In₂O₃ thin films. The structure and crystallinity of the films were investigated by Panalytical Empyrean X-ray Diffractometer (XRD) device (using CuKα1 λ = 1.5405 Å radiation with 2θ of 20–80°, operated at 45 kV and 40 mA). The morphologies of the films were examined by field-emission scanning electron microscope (FE-SEM) images using the FEI Quanta 450 FEG, operated at an acceleration voltage of 20 kV. The chemical compositions of the films were analyzed by EDAX measurements using energy dispersion X-ray spectroscopy (EDAX) analyzer in an FE-SEM system (EDAX, AMETEK Materials Analysis Division).

Using a computer-controlled measurement system that was thoroughly described in our previous studies [18, 20], the gas sensing measurements of In₂O₃ thin film-based sensors were made. The In₂O₃ thin film-based sensors were assessed measuring the resistance change at various CO gas concentrations from 1 ppm to 100 ppm and at different operating temperatures from room temperature to 252 °C. The CO and dry air concentrations in the test chamber were controlled by computer-controlled mass flow controllers (MKS Series). Operating temperatures were controlled using a Lake Shore 325 temperature controller. The current values of the sensors were continuously monitored with a computer-controlled system using the Keithley 2400 sourcemeter and the data were collected in real time using a computer with corresponding data acquisition hardware and software. The relative humidity was kept constant %25 and monitored by a Honeywell HIH-4000 humidity sensor. The sensing response (S) of the sensors is determined via following equation [18];

$$S(\%) = \left(\frac{R_a - R_g}{R_a} \right) \times 100. \quad (1)$$

3 Results and discussion

3.1 Structural, morphological, and compositional analysis

The grazing incidence X-ray diffraction (GIXRD) patterns of In_2O_3 thin films are presented in Fig. 1. The GIXRD patterns of the films indicate the existence of cubic In_2O_3 single phase with a lattice parameter of $a = b = c = 10.11 \text{ \AA}$ and space group: Ia3 [6, 21, 22, JCPDS 98-001-4387] as can be seen in Fig. 1. All the films have a polycrystalline structure that includes orientations along different planes. These planes are (222), (004), and (044). The (222) peak is the strongest, indicating the preferred growth orientation of In_2O_3 cubic structure. Although the full-width at half-maximum (FWHM) and intensity values of these peaks changed with the SILAR cycle number, all the films had the same crystal structure. It was determined that the crystallinity of the films

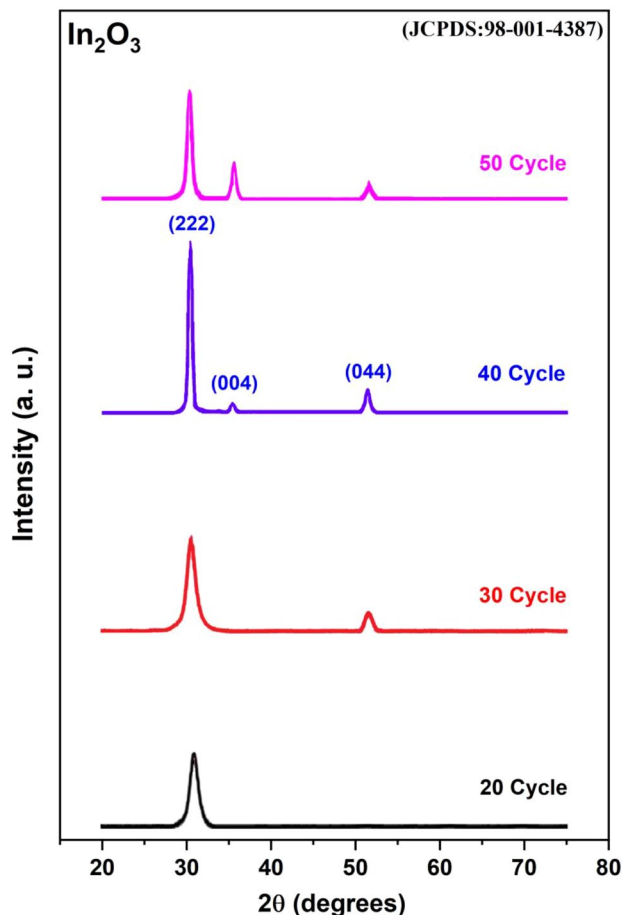


Fig. 1 The GIXRD patterns of In_2O_3 thin films

improved with the cycle number up to 40 SILAR cycle and began to break down after 40 SILAR cycle. In addition, the effect of SILAR cycle on crystallite size and strain values of the films was investigated. The crystallite size (D) of the films was calculated using the β of (222) dominant peak in all the films obtained through the Scherrer's formula [23]:

$$D = \frac{K\lambda}{\beta \cos \theta'} \quad (2)$$

where K is the Scherrer constant (0.9), λ is the used X-ray wavelength, β is the angular line width at half-maximum intensity in radians of the X-ray diffraction dominant peak, and θ is the Bragg's angle. In addition, the strain (s) is calculated using the following equation [23]:

$$s = \frac{\beta \cos \theta}{4}. \quad (3)$$

While, the crystallite size values increase from 9 to 13 nm, strain values decrease from $0.21 \text{ line}^{-2} \text{ m}^{-4}$ to $0.15 \text{ line}^{-2} \text{ m}^{-4}$ with increasing SILAR cycle up to 40, respectively. In 50 SILAR cycle, the crystallite size decreased to 12 nm and the strain value increased to $0.16 \text{ line}^{-2} \text{ m}^{-4}$.

It is very important to determine the surface morphology of metal oxides because the surface properties of metal oxide films used in optoelectronic device applications such as solar cells and gas sensors affect the electrical and optical properties of these devices. FE-SEM images and grain size distributions of In_2O_3 thin films deposited via the SILAR method at 20, 30, 40, and 50 SILAR cycles are presented in Fig. 2. The surface morphology of In_2O_3 -nanostructured thin films has a porous structure composed of small nano-sized particles [24, 25]. As seen in Fig. 2, the homogeneity and density of the films increased, whereas the porosity decreased with increasing SILAR cycle number. Especially, In_2O_3 thin film with 30 SILAR cycle has a homogeneous and uniform surface but a denser porous structure than the others. To determine the grains size, the size distribution of the thin films was plotted by counting the grains in the FE-SEM images via imageJ software. The software-driven grain size values of the In_2O_3 films were determined as 9.18, 11.19, 14.35, and 11.46 nm for 20, 30, 40, and 50 SILAR cycles, respectively. These results obtained from XRD and SEM analysis confirmed a strong correlation between the two measurements.

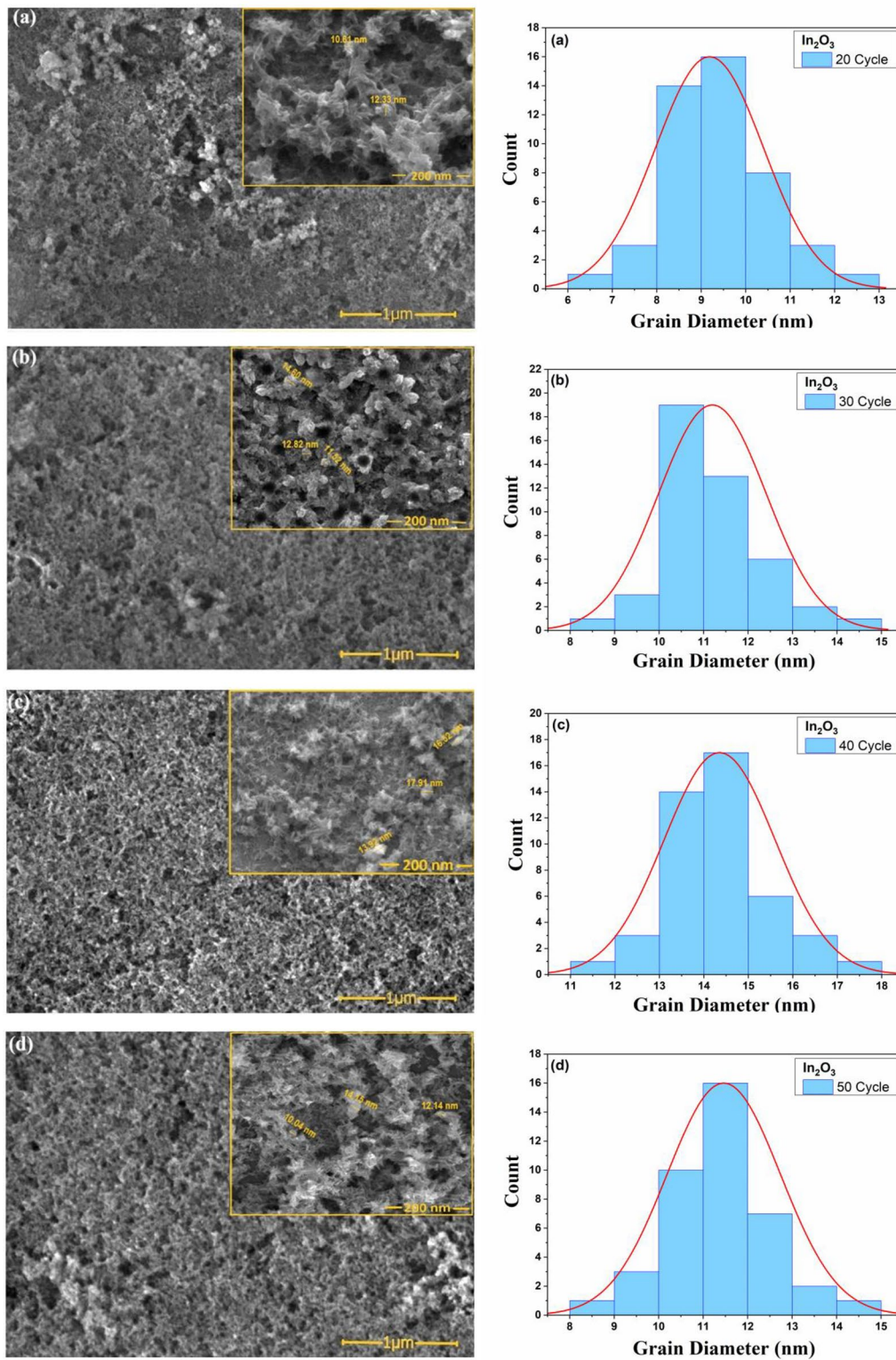


Fig. 2 FE-SEM images and grain size distribution of In_2O_3 thin films [20 SILAR Cycle (a), 30 SILAR Cycle (b), 40 SILAR Cycle (c), and 50 SILAR Cycle (d)]

Previous studies have revealed that porous metal oxide structures had advantage for gas sensor applications as they provided efficient adsorption sites for gas molecules to adsorb and enlarged surface-to-volume ratio for the complete electron depletion and effective gas diffusion, thereby increasing sensor performance. Researchers have focused on the synthesis of In_2O_3 porous structures due to the unique properties of gas sensors based on porous metal oxide structures in recent years [22, 24, 26, 27].

Figure 3 indicates the compositional (EDAX) analysis of In_2O_3 thin films. EDAX analysis revealed the presence of O and In elements in the films. The atomic percent values of these elements in the films were given in the inset of EDAX analysis. The presence of Si element could originate from the substrate. Consequently, the EDAX analysis confirmed that the films were stoichiometrically deposited with SILAR method.

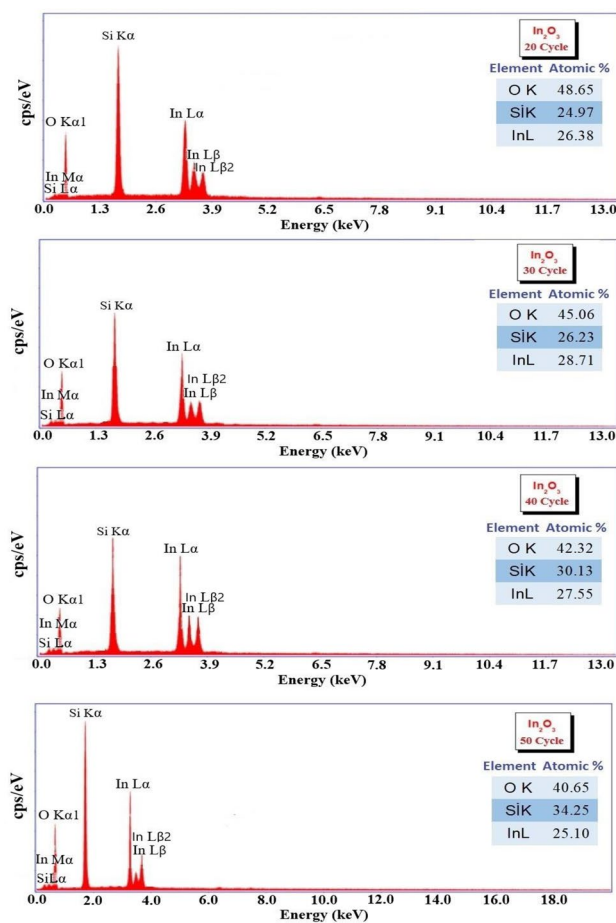


Fig. 3 EDAX analysis of In_2O_3 thin films

3.2 Gas sensing measurements

The plots of electrical resistance (R versus $T(\text{K})$) and $\ln R$ versus $1000/T(\text{K}^{-1})$) of all In_2O_3 thin film-based sensors as a function of operating temperature in dry air are presented in Fig. 4. As seen in Fig. 4; Table 1, it was observed that the resistance values of the sensors decreased with increasing temperature and changed with the SILAR cycle number. This decrease in electrical resistance with increasing temperature in all sensors indicated semiconductor behavior [6]. When the I - V measurement results were investigated, it was determined that this decrease in electrical resistance was because of temperature and not to the diffusion of the Ag metal used as an electrode into the thin films with temperature. Ag material can move or migrate at temperatures above 300°C temperature at the electrode and oxide interface [28]. The temperature-dependent measurements of the sensors were

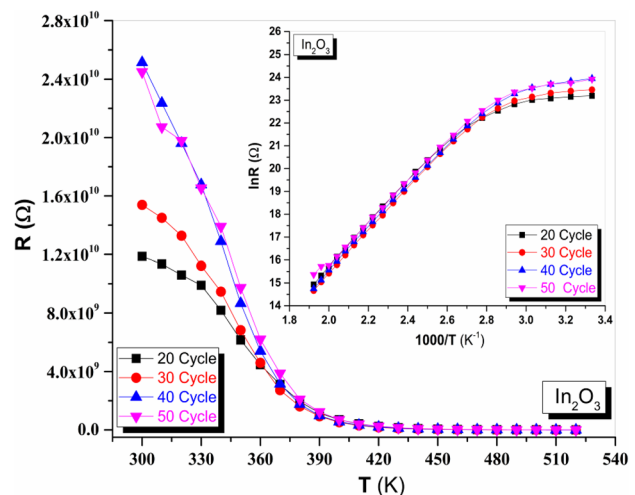


Fig. 4 Behavior of the resistance of the In_2O_3 thin film-based gas sensors versus operating temperature and the plot of $\ln(R)$ versus $1000/T$

Table 1 The resistance (R) and activation energy (E_a) values of In_2O_3 thin film-based gas sensors

In_2O_3 gas sensors	R (Ω)		E_a (eV)	
	300 K	500 K	LR	HR
20 Cycle	1.18×10^{10}	6.79×10^6	0.08	0.700
30 Cycle	1.53×10^{10}	4.98×10^6	0.11	0.735
40 Cycle	2.51×10^{10}	5.73×10^6	0.15	0.749
50 Cycle	2.45×10^{10}	7.00×10^6	0.12	0.703

LR low-temperature region and HR high-temperature region

performed from the room temperature to 252 °C. It is thought that there is no diffusion of Ag material into the thin films since no measurement is taken above 300 °C. Also, the melting point temperature of Ag material is 961.78 °C. Since the measurements of the sensors were not made up to this temperature, it has been thought that diffusion of Ag material into thin films at the atomic scale did not occur. The intrinsic stoichiometric In_2O_3 has insulating properties, and it has high resistivity ($\rho \approx 10^8 \Omega \text{ cm}$) and low free carrier concentration in the close stoichiometric state [29, 30]. The reason for high resistance values of the sensors was attributed to the stoichiometric deposition of In_2O_3 films (as confirmed by EDAX data), dislocations and imperfections in the structure of the films [29–31]. Activation energy (E_a) is one of the important parameters for semiconductor gas sensors. The activation energy was possible to be calculated for two linear regions from the slope of $\ln R$ versus $1000/T$ in Fig. 4 [6]. The E_a values of the sensors were found to change between 0.08 and 0.15 eV at low-temperature region (LR: in the range of 300–340 K) and between 0.700 and 0.749 eV at high-temperature region (HR: in the range of 350–520 K), with SILAR cycle number (in Table 1).

In this study, the effects of SILAR cycle number on CO gas sensing properties of the fabricated In_2O_3 sensors were investigated to optimize the SILAR cycle for a highly sensitive In_2O_3 thin film-based CO gas sensor. For this purpose, CO gas sensing measurements of the sensors as a function of temperature and CO gas concentration were made and the operating temperature and detection limits of the sensors were determined.

Adsorption and desorption of gases on sensing surfaces of sensors or surface reaction of these gases with adsorbed oxygen appears depending upon the operating temperature. Consequently, operating temperature is one of the key parameters in gas sensor applications. To find the optimal operating temperature of the sensors, the temperature-dependent gas sensing measurements were performed from the room temperature to 252 °C at 50-ppm CO gas concentration. Figure 5 indicates the responses of the sensors to 50-ppm CO gas at different operating temperatures. As well known, the operating temperature highly controlled the conductivity, reaction kinetics, and electron mobility and so affected the gas sensing performance of the sensors. When the sensors were operated at temperatures below 87 °C, CO molecules did not have enough thermal energy to react with the surface-adsorbed oxygen species.

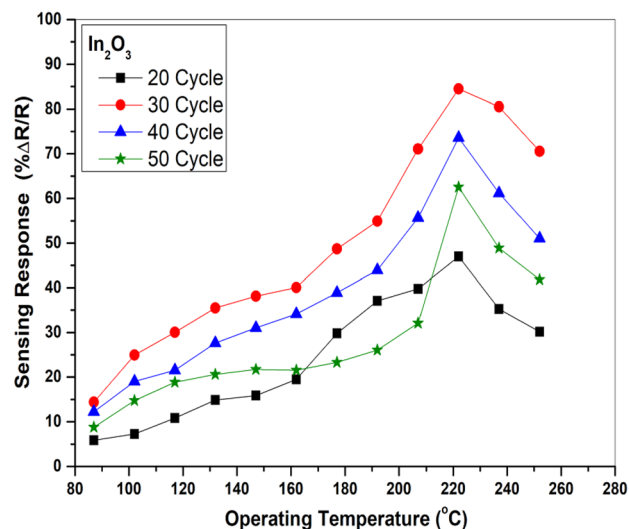


Fig. 5 The sensing responses of In_2O_3 thin film-based gas sensors as a function of operating temperature at 50-ppm CO gas concentration

For this, the responses of the sensors were too low to be detected up to 87 °C. It was noticed from Fig. 5 that the responses of all sensors increased with the operating temperature and reached to the maximum at 222 °C. After this temperature, the responses of all sensors started to decrease. This behavior could be attributed to the kinetic of gas diffusion through the sensing layer and the kinetics of the reaction between CO gas and surface-adsorbed oxygen. As the temperature increased up to 222 °C, the required activation energy for the reaction between the sensor surface and gas molecules decreased and so the response of the sensors increased. However, when the operating temperature was above 222 °C, the CO gas was just consumed at a very shallow surface of the sensing layer, resulting in a decrease in the diffusion depth of the gas. Therefore, the change in sensor resistance decreased and caused decreased responses of the sensors [6, 20, 22, 32, 33]. The optimal operating temperature was found to be 222 °C for all sensors. As seen in Fig. 5, In_2O_3 thin film-based sensor with 30 SILAR cycle had the highest sensitivity for 50-ppm CO gas concentration value at all operating temperatures.

The responses of the sensors to different CO gas concentrations within the range of 1–100 ppm at 222 °C were investigated performing dynamic gas measurements. Figures 6 and 7 indicate dynamic gas measurements of the sensors at 222 °C. The

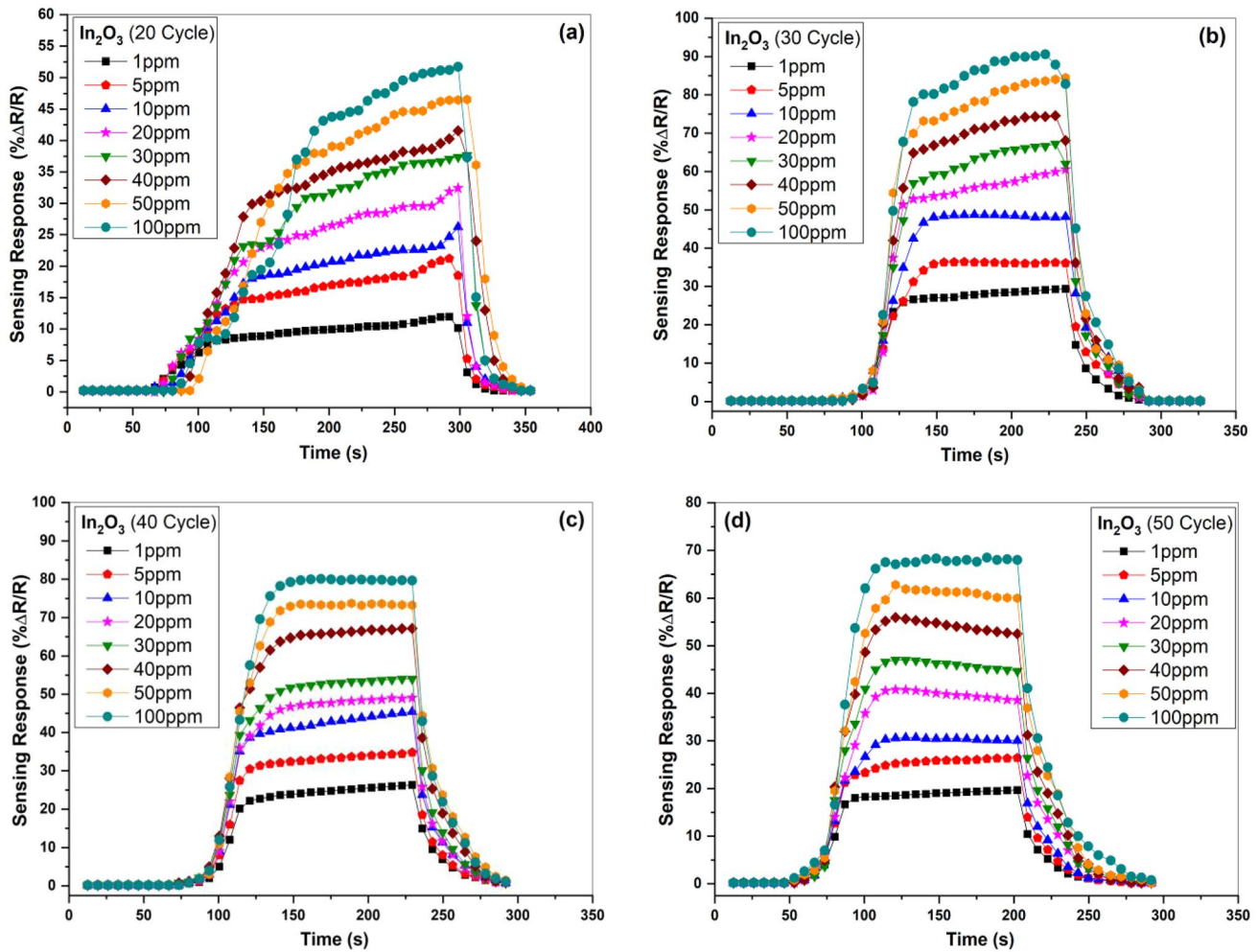


Fig. 6 The time-dependent sensing responses of the In_2O_3 thin film-based gas sensors [20 SILAR Cycle (a), 30 SILAR Cycle (b), 40 SILAR Cycle (c), and 50 SILAR Cycle (d)] toward CO gas at 222 °C

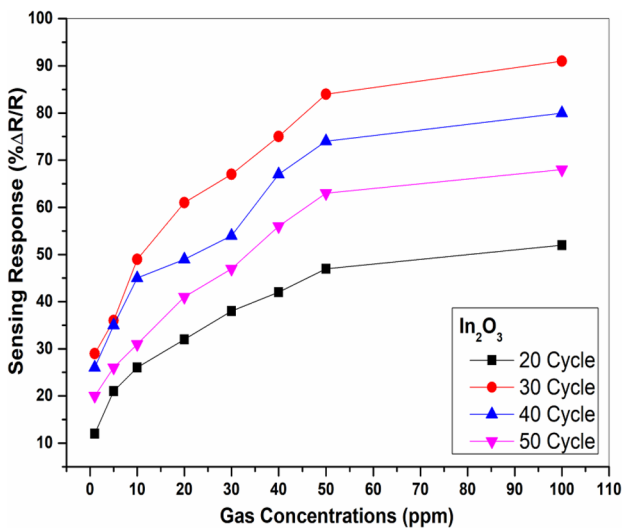


Fig. 7 The sensing responses of the In_2O_3 thin film-based gas sensors as a function of CO gas concentration at 222 °C

responses of the sensors increased with increasing gas concentrations. This behavior was possible to be associated with increased probability of reaction between the surface-adsorbed oxygen species and gas molecules as CO gas concentration increased [6, 12, 18, 22, 27]. As seen in Figs. 6 and 7; Table 2, In_2O_3 thin film-based sensor with 30 SILAR cycle had the maximum response when compared to the other sensors in all CO gas concentrations (within the range of 1–100 ppm) at 222 °C. It was observed for this sensor that the response of the sensor increased from 29 to 91% at 222 °C as the CO gas concentration increased from 1 ppm to 100 ppm. Also, the results revealed that the lowest detection limit for CO gas reached up to 1 ppm at 222 °C with sufficiently high response values for all sensors. The morphological property of this sensor played a crucial role in high response of

Table 2 The sensing responses of In₂O₃ thin film-based gas sensors as a function of gas concentrations at 222 °C

In ₂ O ₃ gas sensors	Sensing response							
	CO gas concentrations							
	1 ppm	5 ppm	10 ppm	20 ppm	30 ppm	40 ppm	50 ppm	100 ppm
20 Cycle	% 12	% 21	% 26	% 32	% 38	% 42	% 47	% 52
30 Cycle	% 29	% 36	% 49	% 61	% 67	% 75	% 84	% 91
40 Cycle	% 26	% 35	% 45	% 49	% 54	% 67	% 74	% 80
50 Cycle	% 20	% 26	% 31	% 41	% 47	% 56	% 63	% 68

the sensor. As indicated in the morphological properties of thin films in Sect. 3.1, it was emphasized that porous metal oxide structures were advantageous for gas sensor applications, thereby increasing the sensor performance. The results proved that the sensor with 30 SILAR cycle with denser porous surface area had the highest response value and the porous nanostructures were a promising sensing material for gas sensor applications. However, few studies were available on the CO gas sensing properties of porous In₂O₃ nanostructures, although porous structures had many advantages. For example, the porous In₂O₃ nanoparticles provided multiple active sites for the adsorption of gas molecules, resulting in a fast sensor response of 6877 for 10-ppm NO₂ gas at a very low temperature of 50 °C [8]. Tong et al. determined that the porous In₂O₃ sensor was the best gas sensing performance at an operating temperature of 350 °C with a response value of approximately

3.5 for 400-ppm CO gas [22]. The mesoporous In₂O₃ nanorod arrays had sensing parameters, such as a response value of 14.9 for 800 ppb NO₂ at 25 °C, a short response time of 14 s, and a short recovery time of 32 s [27]. The porous In₂O₃ nanospheres had a response value of approximately 22 for 100-ppm ethanol at 275 °C [34]. A brief review of In₂O₃-based gas sensors is presented in Table 3.

To evaluate the gas sensing performance of the gas sensors, response and recovery time are two crucial factors. Traditionally, response and recovery times are calculated as the time it takes for the total signal change to reach 90% after the sensor starts interacting with the gas and the time it takes for the total signal change to reach 90% after the interaction ends. However, the shape of the transient signal during the response and recovery phases is critical. When reviewing gas sensor studies in the literature, three different situations regarding the transition

Table 3 Summary of sensing performances of various In₂O₃-based gas sensors

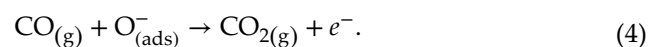
Sensor material	Fabrication method	Target gas	Operation temperature (°C)	Gas concentration (ppm)	Gas response	Response equation	References
In ₂ O ₃	Thermal evaporation	Ethanol	325	1000	10.57	$S = \left(\frac{R_a}{R_a}\right) \times 100$	[6]
In ₂ O ₃	Hydrothermal	NO ₂	50	3	10	$S = \frac{R_g}{R_a}$	[8]
In ₂ O ₃	Hydrothermal	Toluene	220	1	3.55	$S = \frac{R_a}{R_g}$	[12]
In ₂ O ₃	Hydrothermal	CO	350	400	3.5	$S = \frac{R_a}{R_g}$	[22]
In ₂ O ₃	Hydrothermal	H ₂	260	500	18	$S = \frac{R_a}{R_g}$	[24]
InZnO	Sol-gel	CO	300	50	5	$S = \left(\frac{R_a}{R_g}\right) \times 100$	[43]
SnO ₂ /In ₂ O ₃	Electrospinning	CO	200	100	17.45	$S = \left(\frac{R_g - R_a}{R_a}\right) \times 100$	[44]
In ₂ O ₃	SILAR	CO	222	100	91	$S = \left(\frac{R_a - R_g}{R_a}\right) \times 100$	This work

signal are commonly encountered. In the response phase, depending on the on-off periods of the gas, the response may show various behaviors, such as (i) reaching a maximum and saturating (desired state), (ii) reaching a maximum and then falling slowly, or (iii) not reaching the maximum stable value. For signal shapes with all these behaviors, the response and recovery times were calculated by the researchers using the traditional method described above. There is still debate about calculating the recovery time, particularly for signals that are not fully saturated (case iii). It should not be forgotten that an incomplete saturation signal may often be directly related to the on-off time of the gas. Therefore, the estimated response and return times in this special case are the values calculated for the on-off period in the current study [35–40]. Figure 8 indicates the response time and recovery time of In₂O₃ thin film-based sensor with 30 SILAR cycle for 1-ppm and 100-ppm CO gas concentrations at 222 °C. As seen in Fig. 8, the response and recovery times of the sensor with 30 SILAR cycle were found to be 54.2 s and 49 s for 1-ppm CO gas and 47.4 and 62.5 s for 100-ppm CO gas at 222 °C, respectively. The time values were found to be compatible with the reported sensors in the literature [16, 22, 41].

3.3 Gas sensing mechanism

Figure 9 indicates the schematic images of CO sensing mechanism and energy-band diagrams of n-type

In₂O₃ thin film-based sensors [33]. A resistive gas sensor's gas sensing mechanism can be suggested as follows: First, by adsorbing and desorbing oxygen species from the surrounding air on the surface, the electrical behavior is first significantly altered. When exposed to air, the surfaces of porous In₂O₃ thin films will adsorb some oxygen molecules. The oxygen adsorption alters the electrical characteristic of the films. Depending on the operating temperature, the adsorbed oxygen molecules transform into oxygen ions (O₂⁻, O⁻, O²⁻) by capturing free electrons from the conduction band of the films. Thus, a depletion layer is created on the surface regions, which causes an increase in the resistance of the films [22, 33, 42]. When the sensing surface is exposed to CO gas, the adsorbed oxygen ions on the surfaces of the films react with the reducing CO gas [9, 20]. The reaction is indicated as follows [22, 42]:



Electrons are released back into the conduction band of the films, thereby reducing the width of the depletion layer. Consequently, the decrease is observed in the resistance of the films. Tong et al. [22-pages 6–8] and Li et al. [33-pages 172,173] had schematically explained the sensing mechanism of In₂O₃- and Fe₂O₃-based sensors.

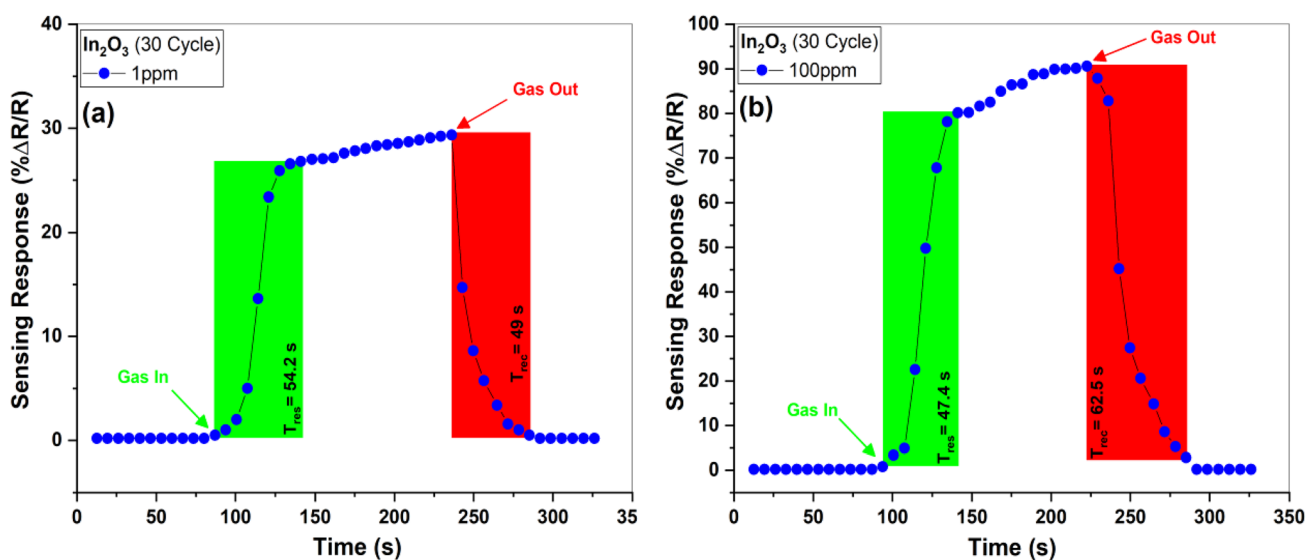
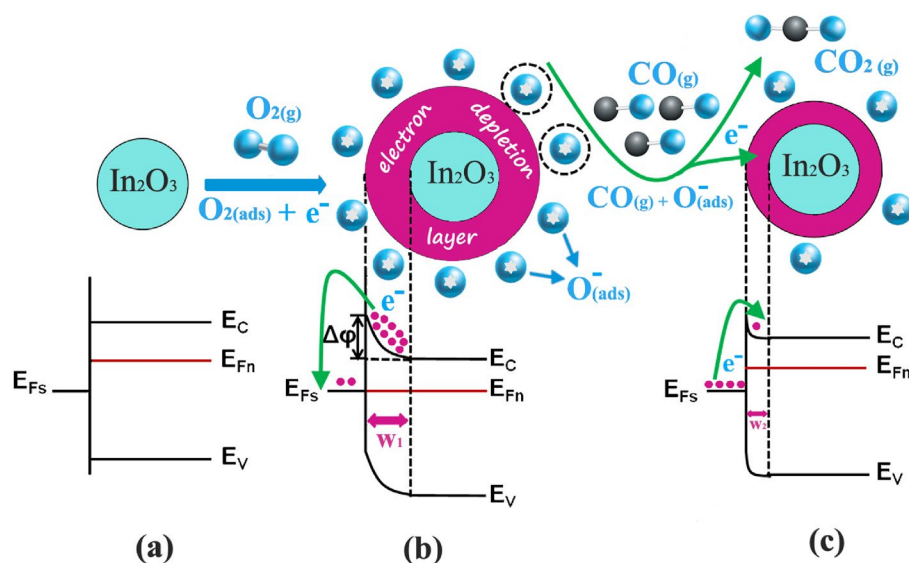


Fig. 8 The response and recovery times of the In₂O₃ thin film-based gas sensor with 30 SILAR cycle for 1-ppm (a) and 100-ppm (b) CO gas concentrations at 222 °C

Fig. 9 Schematic images of the surface reactions and band diagrams of In_2O_3 thin films at different gas atmospheres: **a** in the inert gas atmosphere; **b** in the air atmosphere; and **c** in the reducing CO gas atmosphere



4 Conclusion

In_2O_3 thin films were successfully deposited via SILAR method on glass substrates at 20, 30, 40, and 50 SILAR cycles. The GIXRD results indicated that In_2O_3 thin films had a polycrystalline structure with cubic phase, and the crystallinity of the films improved with the cycle number up to 40 SILAR cycle and then began to break down after 40 SILAR cycle. The surface morphology of the films had a porous structure composed of small nano-sized particles. In_2O_3 thin film with 30 SILAR cycle had a homogeneous and uniform surface but a denser porous structure than the other cycles. The EDAX analysis confirmed that the films were stoichiometrically deposited with SILAR method. The effects of SILAR cycle number on the CO gas sensing properties of the fabricated sensors were investigated as a function of temperature and gas concentration to optimize the SILAR cycle for highly sensitive In_2O_3 thin film-based CO gas sensors. The electrical resistance values of the sensors changed in the range of $1.18 \times 10^{10} - 2.51 \times 10^{10} \Omega$ at 300 K, with SILAR cycle number. The E_a values of the sensors were found to change between 0.08 and 0.15 eV in the range of 300–340 K and between 0.700 and 0.749 eV in the range of 350–520 K, with SILAR cycle number. The SILAR cycle number considerably affected the efficiency of the sensors, according to gas sensing measurements. The CO sensing results indicated that In_2O_3 thin film-based sensor with 30 SILAR cycle had higher sensitivity for 1–100-ppm CO gas concentration values at 222

$^\circ\text{C}$ operating temperature than the other sensors. For this sensor, it was observed that the response of the sensor increased from 29 to 91% at 222 $^\circ\text{C}$ as the CO gas concentration increased from 1 ppm to 100 ppm. The response and recovery times of the sensor with 30 SILAR cycle were found to be 54.2 s and 49 s for 1-ppm CO, and 47.4 and 62.5 s for 100-ppm CO gas at 222 $^\circ\text{C}$, respectively. Consequently, it was revealed how the SILAR cycle number affected the general and CO gas sensing properties of the In_2O_3 thin films, and the SILAR cycle optimization for the highly sensitive In_2O_3 thin-film-based CO gas sensors was determined to be 30 SILAR cycle. In_2O_3 thin film with 30 SILAR cycle was proved to be a promising sensing material for detecting toxic CO gas in air pollution monitoring process.

Author contributions

BH contributed to writing, reviewing, & editing of the manuscript, visualization, methodology, investigation, formal analysis, and conceptualization. STY contributed to writing, reviewing, & editing of the manuscript, methodology, investigation, and conceptualization. BS contributed to writing, reviewing, & editing of the manuscript, and investigation. AA contributed to writing, reviewing, & editing of the manuscript, methodology, investigation, and conceptualization. SA contributed to writing, reviewing, & editing of the manuscript, methodology, investigation, funding acquisition, and conceptualization. MAY contributed

to writing, reviewing, & editing of the manuscript, writing of the original draft, visualization, methodology, investigation, formal analysis, supervision, funding acquisition, and conceptualization.

Funding

Open access funding provided by the Scientific and Technological Research Council of Türkiye (TÜBİTAK). The authors have not disclosed any funding.

Data availability

Data can be made available on reasonable request.

Declarations

Conflict of interest The authors declare that they have no known competing financial interests or personal relationships that could have appeared to influence the work reported in this paper.

Open Access This article is licensed under a Creative Commons Attribution 4.0 International License, which permits use, sharing, adaptation, distribution and reproduction in any medium or format, as long as you give appropriate credit to the original author(s) and the source, provide a link to the Creative Commons licence, and indicate if changes were made. The images or other third party material in this article are included in the article's Creative Commons licence, unless indicated otherwise in a credit line to the material. If material is not included in the article's Creative Commons licence and your intended use is not permitted by statutory regulation or exceeds the permitted use, you will need to obtain permission directly from the copyright holder. To view a copy of this licence, visit <http://creativecommons.org/licenses/by/4.0/>.

References

1. J. Lin, M. Kilani, G. Mao, Recent advances in integrating 1D nanomaterials into chemiresistive gas sensor devices. *Adv. Mater. Technol.* **8**, 2202038 (2023)
2. A. Mirzaei, S. Park, G.J. Sun, H. Kheel, C. Lee, CO gas sensing properties of $\text{In}_4\text{Sn}_3\text{O}_{12}$ and TeO_2 composite nanoparticle sensors. *J. Hazard. Mater.* **305**, 130–138 (2016)
3. R. Nisha, K.N. Madhusoodanan, S. Karthikeyan, A.E. Hill, R.D. Pilkington, NO_2 gas sensing properties of In_2O_3 thin films prepared by pulsed d.c magnetron sputtering technique. *Energy Environ. Focus.* **2**, 157–162 (2013)
4. A. Mirzaeia, S.S. Kim, H.W. Kim, Resistance-based H_2S gas sensors using metal oxide nanostructures: a review of recent advances. *J. Hazard. Mater.* **357**, 314–331 (2018)
5. J. Sun, P. Song, S. Zhang, Z. Sima, Z.C. Lu, Q. Wang, Ag nanoparticles-functionalized dumbbell-shaped In_2O_3 derived from MIL-68(in) with excellent sensitivity to formaldehyde. *J. Alloy Compd.* **888**, 161509 (2021)
6. F. Ghasemi, M. Ghasemi, L. Eftekhari, V. Soleimani, Comparison and influence of metal dopants on the optoelectrical, microstructure and gas sensing properties of nanostructured indium oxide films. *Opt. Laser Technol.* **146**, 107564 (2022)
7. Z.G. Zhang, X.X. Wang, J. Zhang, M. Yu, J.C. Zhang, H.D. Zhang, Y.Z. Long, Recent advances in 1D micro- and nanoscale indium oxide structure. *J. Alloy Compd.* **752**, 359–375 (2018)
8. S.P. Patil, V.L. Patil, S.A. Vanalakar, S.S. Shendage, S.A. Pawar, J.H. Kim, J. Ryu, D.R. Patil, P.S. Patil, Porous In_2O_3 thick films as a low temperature NO_2 gas detector. *Mater. Lett.* **306**, 130916 (2022)
9. K. Inyawilert, A. Wisitsora-at, A. Tuantranont, P. Singjai, S. Phanichphant, C. Liewhiran, Ultra-rapid VOCs sensors based on sparked- In_2O_3 sensing films. *Sens. Actuators B Chem.* **192**, 745–754 (2014)
10. C.W. Lai, J.Y. Dai, X.Y. Zhang, H.L.W. Chan, Y.M. Xu, Q. Li, H.C. Ong, In situ synthesis and phase transformation of $\text{In}_2\text{O}_3/\text{Sb}$ core-shell nanostructures. *J. Cryst. Growth.* **282**, 383–388 (2005)
11. D.L. Shao, L.Q. Qin, S. Sawyer, Near ultraviolet photo-detector fabricated from polyvinyl-alcohol coated In_2O_3 nanoparticles. *Appl. Surf. Sci.* **261**, 123–127 (2012)
12. X. Liu, X. Duan, C. Zhang, P. Hou, X. Xu, Improvement toluene detection of gas sensors based on flower-like porous indium oxide nanosheets. *J. Alloy Compd.* **897**, 163222 (2022)
13. L.L. Zheng, T.T. Ma, Y.Q. Zhao, Y.S. Xu, L. Sun, J. Zhang, X.H. Liu, Synergy between Au and In_2O_3 microspheres: a superior hybrid structure for the selective and sensitive detection of triethylamine. *Sens. Actuators B Chem.* **290**, 155–162 (2019)
14. Y. Wang, X. Sun, J. Cao, Enhanced methane sensing performance of Ag modified In_2O_3 microspheres. *J. Alloy Compd.* **895**, 162557 (2022)

15. G.N. Gerasimov, M.I. Ikim, V.F. Gromov, O.J. Ilegbusi, L.I. Trakhtenberg, Chemical modification of impregnated SnO₂-In₂O₃ nanocomposites due to interaction of sensor components. *J. Alloy Compd.* **883**, 160817 (2021)
16. S.P. Ratnayake, J. Ren, E. Colusso, M. Guglielmi, A. Martucci, E.D. Gaspera, SILAR deposition of metal oxide nanostructured films. *Small.* **17**, 2101666 (2021). <https://doi.org/10.1002/sml.202101666>
17. H. Soonmin, M.B. Tahir, S.N. Das, M.R. Das, Preparation of thin films by SILAR and spin coating method. *Eurasian J. Anal. Chem.* ISSN: 1306–305, <https://www.researchgate.net/publication/338736850>
18. B. Soltabayev, M.A. Yıldırım, A. Ateş, S. Acar, The effect of indium doping concentration on structural, morphological and gas sensing properties of IZO thin films deposited SILAR method. *Mater. Sci. Semicond. Process.* **101**, 28–36 (2019)
19. B. Soltabayev, A.O. Çağırtekin, A. Mentbayeva, M.A. Yıldırım, S. Acar, Investigation of indium insertion effects on morphological, optical, electrical impedance and modulus properties of ZnO thin films. *Thin Solid Films.* **734**, 138846 (2021)
20. I. Karaduman, M.A. Yıldırım, S.T. Yıldırım, A. Ateş, Y.A. Özdemir, S. Acar, The effect of different doping elements on the CO gas sensing properties of ZnO nanostructures. *J. Mater. Sci: Mater. Electron.* **28**, 18154–18163 (2017)
21. N. Beji, M. Reghima, M. Souli, N.K. Turki, Effect of nitrogen annealing on the structural, optical and photoluminescence properties of In₂O₃ thin films. *J. Alloy Compd.* **675**, 231–235 (2016)
22. P.V. Tong, L.H. Minh, N.V. Duy, C.M. Hung, Porous In₂O₃ nanorods fabricated by hydrothermal method for an effective CO gas sensor. *Mater. Res. Bull.* **137**, 111179 (2021)
23. M.A. Yıldırım, Y. Akaltun, Ateş, characteristics of SnO₂ thin films prepared by SILAR. *Solid State Sci.* **14**, 1282–1288 (2012)
24. Z. Li, S. Yan, Z. Wu, H. Li, J. Wang, W. Shen, Z. Wang, Y. Fu, Hydrogen gas sensor based on mesoporous In₂O₃ with fast response/recovery and ppb level detection limit. *Int. J. Hydrogen Energy.* **43**, 22746–22755 (2018)
25. D. Craciun, P. Garoi, M. Mogildea, G. Mogildea, S.I. Zgura, B.S. Vasile, V. Craciun, Crystalline In₂O₃ nanoparticles synthesis using microwaves vaporization of metallic wires. *Appl. Surf. Sci.* **575**, 151788 (2022)
26. T. Wagner, C.D. Kohl, S. Morandi, C. Malagù, N. Donato, M. Latino, G. Neri, M. Tiemann, Photoreduction of mesoporous In₂O₃: mechanistic model and utility in gas sensing. *Chem. Eur. J.* **18**, 8216–8223 (2012)
27. Y. Shen, X. Zhong, J. Zhang, T. Li, S. Zhao, B. Cui, D. Wei, Y. Zhang, K. Wei, In-situ growth of mesoporous In₂O₃ nanorod arrays on a porous ceramic substrate for ppb-level NO₂ detection at room temperature. *Appl. Surf. Sci.* **498**, 143873 (2019)
28. S.P. Lee, Electrodes for Semiconductor Gas Sensors. *Sensors.* **17**, 4 (2017). <https://doi.org/10.3390/s17040683>
29. A.A. Dakhel, Effect of ytterbium doping on the optical and electrical properties of intrinsic In₂O₃ thin films. *Microelectron. Reliab.* **50**, 211–216 (2010)
30. S. Guo, L. Yang, X. Zhangd, B. Dai, F. Geng, Z. Yang, P. Wang, G. Gao, L. Xu, J. Han, V. Ralchenko, J. Zhua, Modulation of optical and electrical properties of In₂O₃ films deposited by high power impulse magnetron sputtering by controlling the flow rate of oxygen. *Ceram. Int.* **45**, 21590–21595 (2019)
31. Y. Akaltun, M.A. Yıldırım, A. Ateş, M. Yıldırım, The relationship between refractive index-energy gap and the film thickness effect on the characteristic parameters of CdSe thin films. *Opt. Commun.* **284**, 2307–2311 (2011)
32. D. Vernardou, M. Apostolopoulou, D. Louloudakis, N. Katsarakis, E. Koudoumas, Hydrothermally grown β-V₂O₅ electrode at 95 °C. *J. Colloid Interface Sci.* **424**, 1–6 (2014)
33. Z. Li, Y. Huang, S. Zhang, W. Chen, Z. Kuang, D. Ao, W. Liu, Y. Fu, A fast response & recovery H₂S gas sensor based on α-Fe₂O₃ nanoparticles with ppb level detection limit. *J. Hazard. Mater.* **300**, 167–174 (2015)
34. P. Song, D. Han, H. Zhang, J. Li, Z. Yang, Q. Wang, Hydrothermal synthesis of porous In₂O₃ nanospheres with superior ethanol sensing properties. *Sens. Actuators B Chem.* **196**, 434–439 (2014)
35. N.A. Isaac, I. Pikaar, G. Biskos, Metal oxide semiconducting nanomaterials for air quality gas sensors: operating principles, performance, and synthesis techniques. *Microchim. Acta.* **189**, 196 (2022)
36. M.A. Basyooni, M. Shaban, A.M. El, Sayed, Enhanced gas sensing properties of spin-coated Na-doped ZnO nanostructured films. *Sci. Rep.* **7**, 41716 (2017)
37. I.Y. Habib, A.A. Tajuddin, H.A. Noor, M.C. Lim, A.H. Mahadi, N.T.R.N. Kumara, Enhanced carbon monoxide-sensing properties of chromium-doped ZnO nanostructures. *Sci. Rep.* **9**, 9207 (2019)
38. G. Dubourg, A. Segkos, J. Katona, M. Radovic, S. Savic, G. Niarchos, C. Tsamis, Crnojevic-Bengin, fabrication and characterization of flexible and miniaturized humidity sensors using screen-printed TiO₂ nanoparticles as sensitive layer. *Sensors.* **17**, 1854 (2017)
39. P. Chaudhary, A. Singh, S. Sikarwar, B.C. Yadav, One-pot synthesis of phosphine-free indium selenide (InSe) QDs and their structural characterization for LPG and humidity sensing. *J. Mater. Sci. Mater. Electron.* **33**, 11802–11812 (2022)

40. T. Wang, J. Hao, S. Zheng, Q. Sun, D. Zhang, Y. Wang, Highly sensitive and rapidly responding room-temperature NO₂ gas sensors based on WO₃ nanorods/sulfonated graphene nanocomposites. *Nano Res.* **11**, 791–803 (2018)
41. A. Qurashi, E.M. El-Maghraby, T. Yamazaki, T. Kikuta, Catalyst supported growth of In₂O₃ nanostructures and their hydrogen gas sensing properties, *Sens. Actuators B Chem* **147**, 48–54 (2010)
42. K. Wetchakun, T. Samerjai, N. Tamaekong, C. Liewhiran, C. Siriwong, V. Kruefu, A. Wisitsoraat, A. Tuantranont, S. Phanichphant, Semiconducting metal oxides as sensors for environmentally hazardous gases. *Sens. Actuators B Chem* **160**, 580–591 (2011)
43. R. Dhahri, M. Hjiri, L. El Mir, H. Alamri, A. Bonavita, D. Iannazzo, S.G. Leonardi, G. Neri, CO sensing characteristics of In-doped ZnO semiconductor nanoparticles. *J. Sci. : Adv. Mater. Dev.* **2**, 34–40 (2017)
44. K.-C. Hsu, T.-H. Fang, I.-T. Tang, Y.-J. Hsiao, C.-Y. Chen, Mechanism and characteristics of Au-functionalized SnO₂/In₂O₃ nanofibers for highly sensitive CO detection. *J. Alloys Compd.* **822**, 153475 (2020)

Publisher's Note Springer Nature remains neutral with regard to jurisdictional claims in published maps and institutional affiliations.